

Supporting Information for

The role of MAPbI₃ hydrate in Triple Mesoscopic Stack Minimodules: The Key to Elongating Outdoor Lifespan.

Susana Iglesias-Porras^{†}, Amy Neild[†], Johannes Gausden^{††}, Mathew Barraclough^{††}, Elizabeth A. Gibson^{†*}.*

[†]Energy Materials Laboratory, School of Natural and Environmental Science, Newcastle University, Newcastle Upon Tyne, NE1 7RU, UK.

^{††}School of Engineering Newcastle University, Newcastle Upon Tyne, NE1 7RU, UK

Contents

Section 1. Experimental methods	2
Section 2. Outdoor testing rig	5
Section 3. Device performance	8
Section 4. Data processing	11
Section 5. Parylene-C deposition: effect on devices.....	14
Section 6. AFM Images.	16
Section 7. Environmental Conditions.	17
Section 8. V _{OC} -to-RH relationship.....	19
Section 9. Lab Hydration and Dehydration experiments.....	28
References.....	33

Section 1. Experimental methods

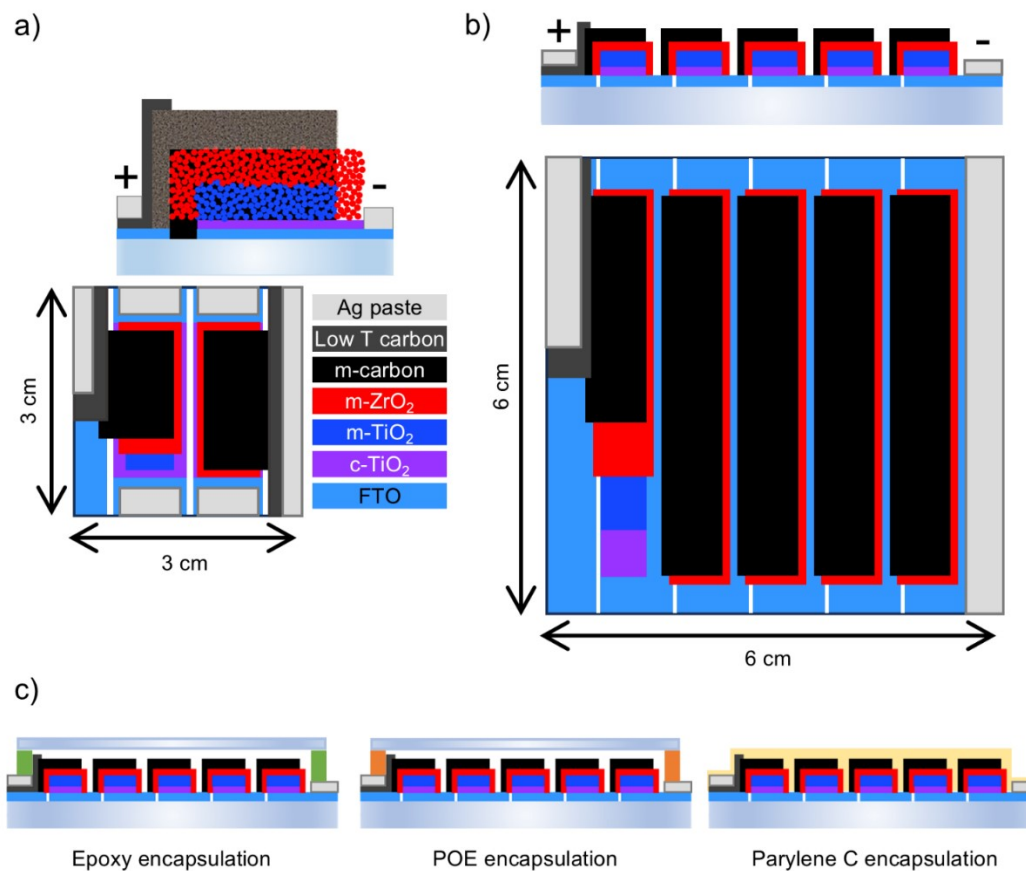


Figure S 1. Device architecture for perovskite triple mesoscopic stack solar cells (a) and minimodules (b), and encapsulation architectures (c).

Material	Water Vapor Transmission Rate [g/m ² /day]	Thermal Degradation Threshold (in air) [°C]	Notes
Epoxy	~0.2* ¹	~80 ²	Brittle above thermal threshold
POE	~4-5* ¹	~75-95 ³	Flexible, more prone to water ingress
Parylene-C	~0.008** ⁴	~125*** ⁵	Excellent barrier against moisture ingress. Can survive 10 years @ 80°C in air. ⁵

Table S 1. Summary of water vapor transmission rates and thermal degradation thresholds for encapsulation materials used in this study

* Measured at 23°C, 85% RH. Given in for a 100 µm thick film; ** Measured at 37°C, 90% RH. Given for a 100 µm thick film.; *** T5 point (modulus = 690 MPa)

Sample	Temperature	Pressure	Time
AN014-04	90 °C	100 mbar	20 min
AN014-06		200 mbar	20 min
AN014-09		100 mbar	10 min

Table S 2. POE encapsulation conditions used in laminator.

Minimodule	Illuminated Area (cm²)
SIP045-I	10.35
AN014-04	12.39
AN014-06	12
AN014-09	11.79
AN014-12	11.79
SIP053-09	14.4
AN013-11	13.5
SIP053-03	14.4
AN012-a-03	13.65
AN012-a-04	13.65

Table S 3. Masked areas for minimodules.

Note that samples AN013-11, SIP953-03, AN012-a-03 and AN012-a-04 were left unmasked to be able to see the degradation products more clearly from the glass side (thus illuminated area equals active area in this case).

Section 2. Outdoor testing rig

The solar cell testing equipment was comprised of two main components: a testing rig subdivided in a top and bottom box containing the measuring equipment, and a tiltable metal frame designed to hold the solar cells, mini-modules, panels, and electronic boxes, as showcased in Figure S 2(a).

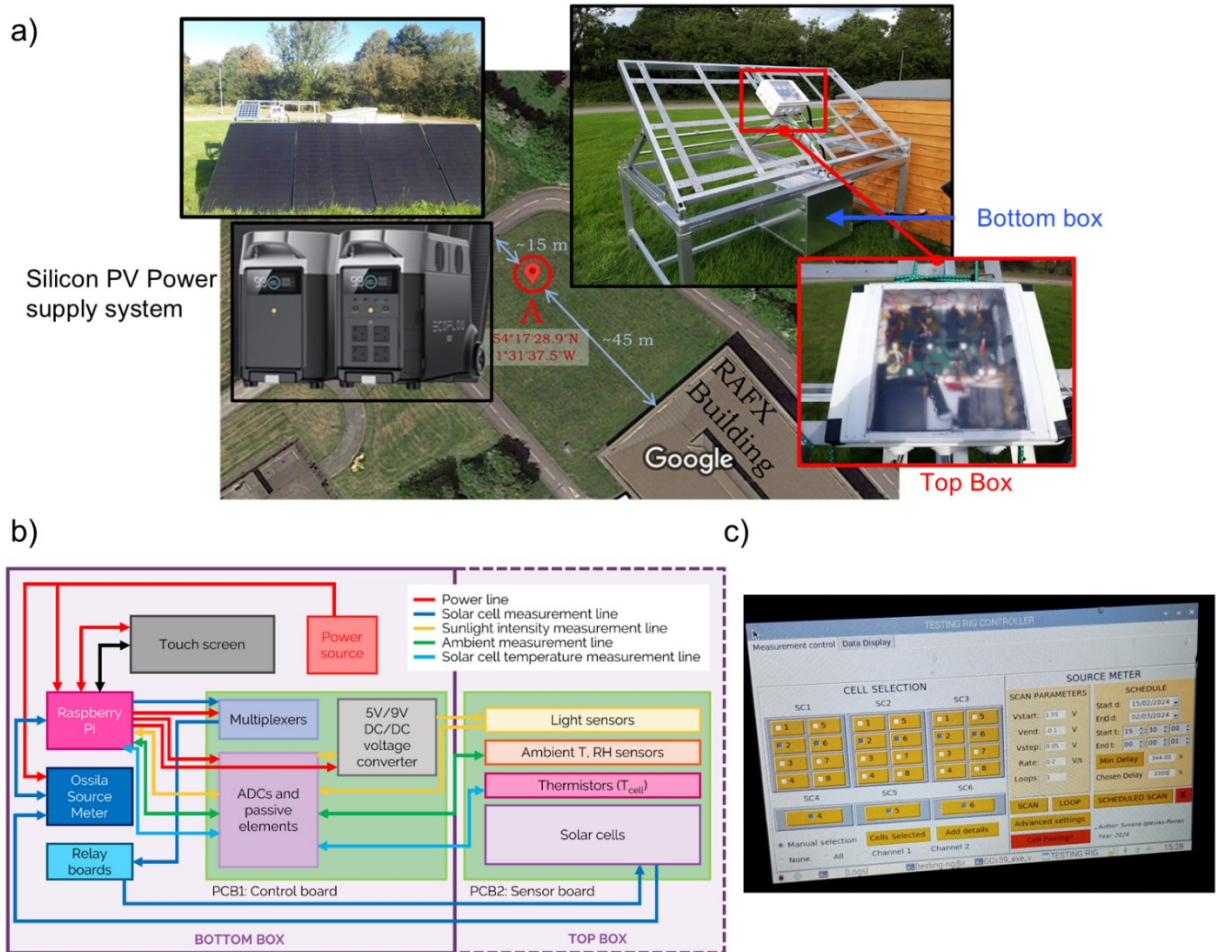


Figure S 2. Scheme of outdoor testing parts (a), internal circuitry (b), and in-house designed software (c).

Solar cells and minimodules were connected to the system through the top box, which was equipped with sensors able to capture the temperature of the cell, ambient humidity and temperature, and light intensity. The system allowed for the measurement of multiple lab-scale devices: small cells containing 8 solar cells per substrate, medium cells containing 2 solar cells per substrate, and minimodules. Solar cell power was assessed through JV scans executed by a source meter located in the bottom box and

commanded by a Raspberry Pi with a touch screen. The collected data was stored in the SD card of the Raspberry Pi and automatically uploaded to the cloud via connection with a local 5G network.

The electronic components of the measuring system were interconnected through two printed circuit boards (*PCB1: Control board* and *PCB2: Sensor board*) located at the bottom and top box and joined via ribbon cables. The main power was fed to the source meter and the Raspberry Pi via a standard 220V, 50 Hz line connection from the portable power station connected to a 1.6 kW commercial silicon system. The Raspberry Pi controlled four measurement lines as depicted in Figure S 2(b). The solar cell measuring line (dark blue) connected each cell to the source meter via relays and multiplexers, enabling JV scans upon user command. The sunlight intensity measurement line (yellow) captured sunlight using photodiodes (OSRAM BPW21) with an amplifier boosting the signal before conversion by an analog-to-digital converter (ADC). The photodiodes were previously calibrated against the AM 1.5 G spectrum in the solar simulator between 0 and 1 suns. To do so, light intensity was fixed at 1 sun and lower intensities were achieved with a reflective neutral density filter kit. Calibration scans fitted to a biexponential can be found in Figure S 3. The OSRAM BPW21 spectral sensitivity range is 350–820 nm, with a peak response at 550 nm, well matched to the perovskite devices absorption range (~300–800 nm). We note that differences in angular response between the sensor and measured devices, both lacking cosine correction, may cause minor variations in J_{sc} measurements, especially under diffuse or low-angle light. The ambient measurement line (green) collected temperature and humidity data via DHT22 sensors, while the solar cell temperature measurement line (light blue) used thermistors (ATC Semitec 103JT-025 Jt) attached to the cells, converting resistance changes to digital data via the ADC.

To enable the operation outdoors both the top and bottom boxes comply with an IP65 standard, offering full protection against dust ingress and against low pressure jets of water from all directions. Electronic connections between boxes were protected through grey nylon cable glands rated to an IP68 and parallel corrugated nylon conduits. Additionally, the top box incorporated a transparent plastic window made of Perspex with an Anti-reflective coating to reduce light transmission losses. Although efforts were made

to keep air circulation within the box through lateral openings, overheating occurred especially on sunny days, prompting the registers of ambient and cell temperature to spike towards abnormally high values as detailed in Figure S 10.

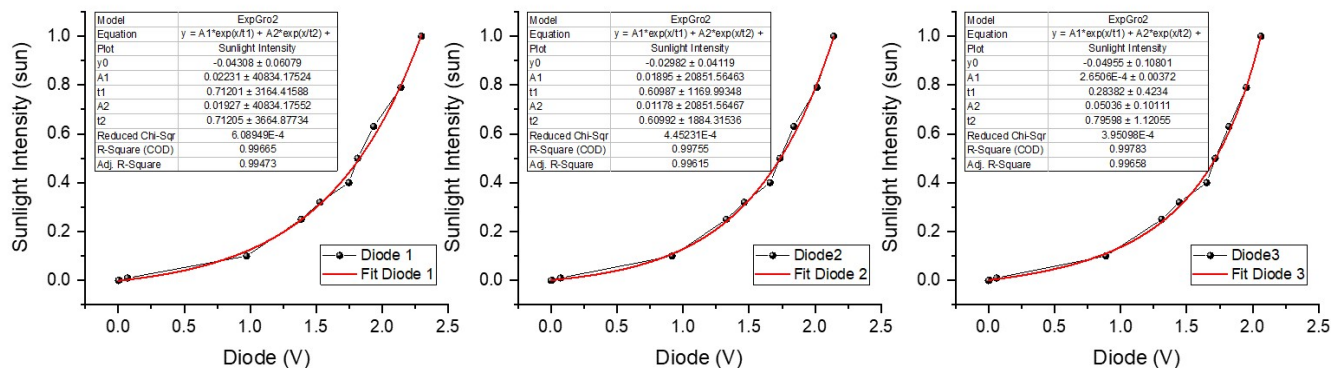


Figure S 3. Photodiodes sunlight calibration plots.

The measuring program was controlled through the in-house designed and built Python application depicted in Figure S 2(c). The application allows the user to select which solar cells to measure, add details of the solar cells, modify the JV scan parameters, and start the data collection either executing the measurements manually (Scan and Loop) or scheduling the rig to start the measurement at a specific date and time (Scheduled Scan). Scheduled scans were designed to measure from sunrise to sunset exclusively at a rate of 0.2 V s^{-1} only recording the reverse scans. This limitation in the number of measurements was made to preserve the charge in the batteries of the silicon power supply system.

Collected data was automatically saved in the Raspberry Pi in using two types of text files: Log files and JV scan files. A Log file was created and saved every time the user executed a measurement, including a record of the date, time, solar cell details (Cell ID, Sample ID, Area, Variables 1-3), a summary of the main solar cell parameters extracted from the JV scan (PCE, J_{SC} , V_{OC} , FF, R_{series} , R_{shunt}), the location path of the JV scan file and sensor data (cell temperature, ambient humidity, ambient temperature, sunlight intensity) for each scanned solar cell. JV scan files contained the voltage sweep and the corresponding current densities generated by the device.

Section 3. Device performance

In this paper, we analysed a total of 16 samples. This section presents the stabilised scan parameters of the solar cells and minimodules fabricated under 1 sun (Table S 4), explaining their modest efficiency due to various factors. These samples were produced in different batches, with those selected for outdoor testing originally representing the highest-performing cells in their respective batches. Samples from the same batch share a common code before the hyphen, while the number after the hyphen identifies the specific cell. Additionally, we define the "initial" state as the respective starting point of each hydration experiment, whether conducted indoors or outdoors.

The final power conversion efficiency (PCE) results were obtained after stabilization through light soaking. JV scans in the reverse direction were performed until efficiency gains were less than 0.01%, at which point a forward scan was conducted. Throughout this publication, we primarily plotted the reverse scans, as our main focus is on comparing the hydrated state to the initial state. This ensures consistency with outdoor testing rig measurements (only taken in the reverse) and prevents overpopulation of the graphs, making them easier to interpret. However, we include forward scan values in this section and in the calibration plots (Figure S 4) to highlight their differences and acknowledge the presence of hysteresis.

Several factors contributed to the modest efficiency of the devices. One key reason is that some of the solar cells were already a few months old before the experiment began, which may have led to a decline in performance compared to their fresh state. However, this does not impact the validity of our comparisons, as we are analysing hydration effects relative to each cell's initial condition within the experiment—not its original manufacturing state. To account for this, we have marked the affected cells in Table S 4 with a star (*).

Sample	Type	Reverse scan				Forward Scan			
		PCE (%)	J _{sc} (mA cm ⁻²)	V _{oc} (V)	FF	PCE (%)	J _{sc} (mA cm ⁻²)	V _{oc} (V)	FF
SIP045-I	Minimodule	4.237	2.115	3.846	0.521	3.367	2.041	3.739	0.441
AN006-12L	Solar cell	3.43	12.721	0.681	0.396	2.884	11.784	0.663	0.369
AN014-04	Minimodule	6.897	3.567	3.87	0.500	4.680	3.391	3.441	0.401
AN014-06	Minimodule	7.483	3.779	3.822	0.518	6.319	3.668	3.576	0.482
AN014-09	Minimodule	7.824	4.168	3.991	0.47	6.220	3.969	3.545	0.442
AN014-12	Minimodule	5.961	3.219	4.028	0.46	4.674	3.101	3.683	0.409
SIP053-09	Minimodule	5.272	2.498	3.942	0.535	4.232	2.437	3.878	0.448
AN013-11*	Minimodule	3.106	1.555	3.434	0.582	1.886	1.485	3.421	0.371
SIP053-03	Minimodule	2.153	1.43	3.415	0.441	1.987	1.395	3.38	0.421
AN012-a-03*	Minimodule	3.04	2.437	3.521	0.354	2.091	2.338	3.515	0.254
AN012-a-04*	Minimodule	5.873	3.049	3.812	0.505	4.95	2.954	3.817	0.439
SIP058-01R	Solar cell	3.094	13.263	0.709	0.329	2.579	12.582	0.677	0.303
SIP058-02R	Solar cell	3.01	9.552	0.753	0.419	2.261	8.354	0.702	0.385
SIP058-04L	Solar cell	4.189	15.499	0.67	0.403	3.743	14.576	0.664	0.386
SIP058-05R	Solar cell	2.768	8.431	0.733	0.448	2.602	7.946	0.728	0.45
SIP058-12R	Solar cell	1.631	3.877	0.751	0.561	1.572	3.803	0.741	0.558

Table S 4. Stabilized reverse and forward cell parameters of all solar cells and minimodules.

The devices generally showcased lower efficiencies compared to similar reports in the literature, which we attribute to suboptimal fabrication conditions. Manual spray and screen-printing processes introduced cumulative errors, particularly after the glass was cut. Imperfectly cut glass caused misalignments in the laser etcher and subsequent screen-printing layers, sometimes leading to shunts. Furthermore, high series resistance effects, commonly observed in triple mesoscopic stacks, also contributed to efficiency losses. These effects stem from the engineering of the mesoporous layers, where factors such as surface roughness, defects at mesoporous interfaces, excessive layer thickness, and variations in pore size can

significantly increase series resistance. Optimizing these layers in the future could help lower sheet resistance and enhance overall device performance.

Additionally, the slot-die coating process posed challenges, as the coater often failed to distribute solution volumes accurately. This resulted in uneven perovskite deposition and patchy infiltration, a problem that was particularly evident in SIP045-I—part of the first minimodule batch we fabricated—where some stripes were not fully infiltrated. This issue manifested as a highly irregular JV scan, as shown in Figure S 4. Likewise, the drying conditions for the perovskite posed another source of variability. Despite using a relatively homogeneous hotplate, drying was affected by uncontrollable factors such as high airflow within the fume hood.

For the minimodules, efficiency was further limited by the relatively large spacing—approximately 2-3 mm—between individual cells. This gap represents the distance between the carbon layer and the FTO of the adjacent stripe. Since FTO is not highly conductive, reducing this gap or incorporating bus bars could help mitigate losses. This issue likely explains why we did not reach the expected voltage of 4.5-5 V, assuming an individual stripe voltage of 0.9-1 V, which in turn translates to lower efficiencies. Future work will focus on reducing this gap to improve performance. The current design resulted from reusing masks originally made for small cells, which influenced the spacing in the minimodules.

Section 4. Data processing

The outdoor data was processed using a custom Python script. Before deployment, the solar cells were tested in the solar simulator at light intensities ranging from 0.1 to 1 sun, where JV scans were recorded, and key parameters (PCE, J_{SC} , V_{OC} , FF) were extracted for each intensity, generating a calibration file. Calibration measurements for the outdoor deployed cells can be found in Figure S 4 (JV scans) and Figure S 5 (Cell parameters).

The Python script then analyzed the log file from the outdoor tests, retrieving light intensity values and using the calibration file to predict power and other cell parameters via Akima interpolation. The percentage change between the predicted and observed J_{SC} and V_{OC} values was calculated by dividing the observed values by the interpolated predicted values and multiplying by 100.

Faulty records were removed, such as cases where JV scans indicated a disconnected cell, and erroneous relative humidity (RH) measurements exceeding 100% were corrected by substituting values from an adjacent cell measured within a two-minute window.

The surface temperature (T_{cell}) of the SIP045-I minimodule exhibited significantly and consistently lower values compared to the other cells in the box, indicating insufficient attachment of the thermistor to the sample surface. Since all samples shared the same black color, we corrected the T_{cell} measurements for SIP045-I by averaging the T_{cell} values of the adjacent cells that were measured at the same time.

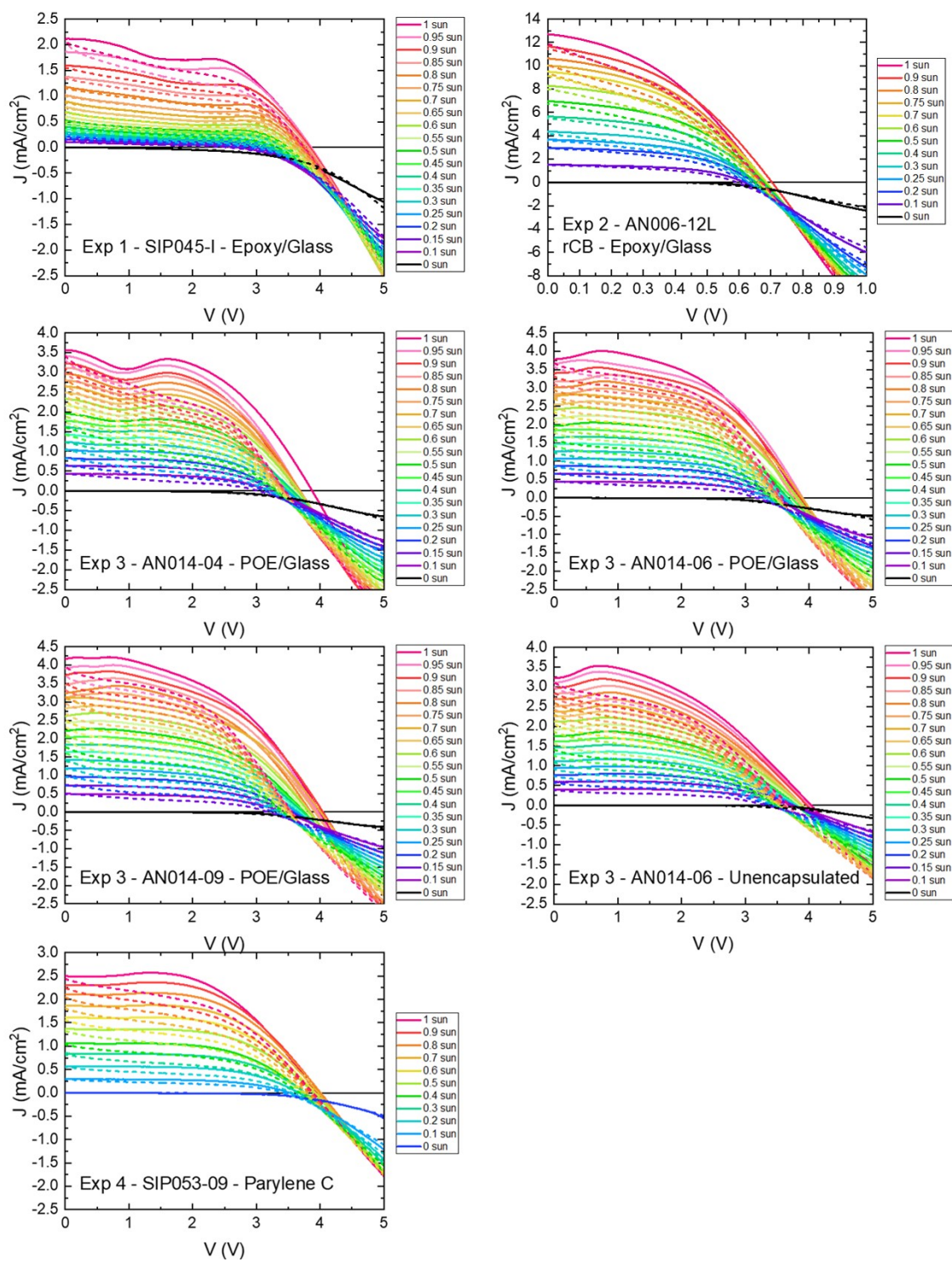


Figure S 4. Reverse (solid line) and forward (dashed line) JV calibration scans taken before outdoor deployment of TMS devices between 0.1 and 1 sun.

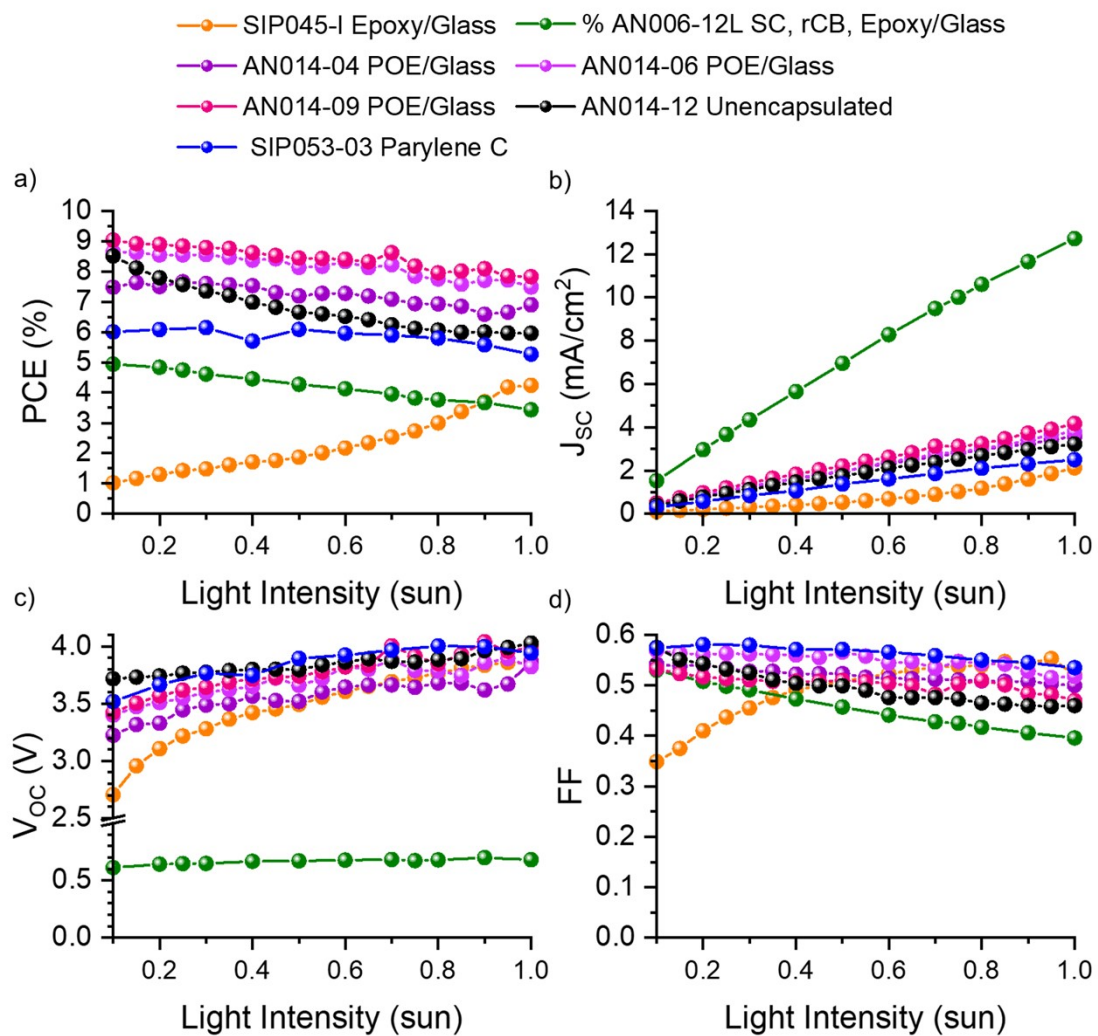


Figure S 5. Reverse cell parameters of TMS devices taken before outdoor deployment between 0.1 and 1 sun.

Section 5. Parylene-C deposition: effect on devices.

In this section, we highlight the uniform, pinhole-free coverage of the 10-micron Parylene-C layer (Figure S 6) in contrast to the appearance of the bare device (Figure S 7). Additionally, Figure S 8 demonstrates that there is minimal change in performance and JV scans before and after deposition, confirming that the Parylene-C layer does not negatively impact the device's functionality.

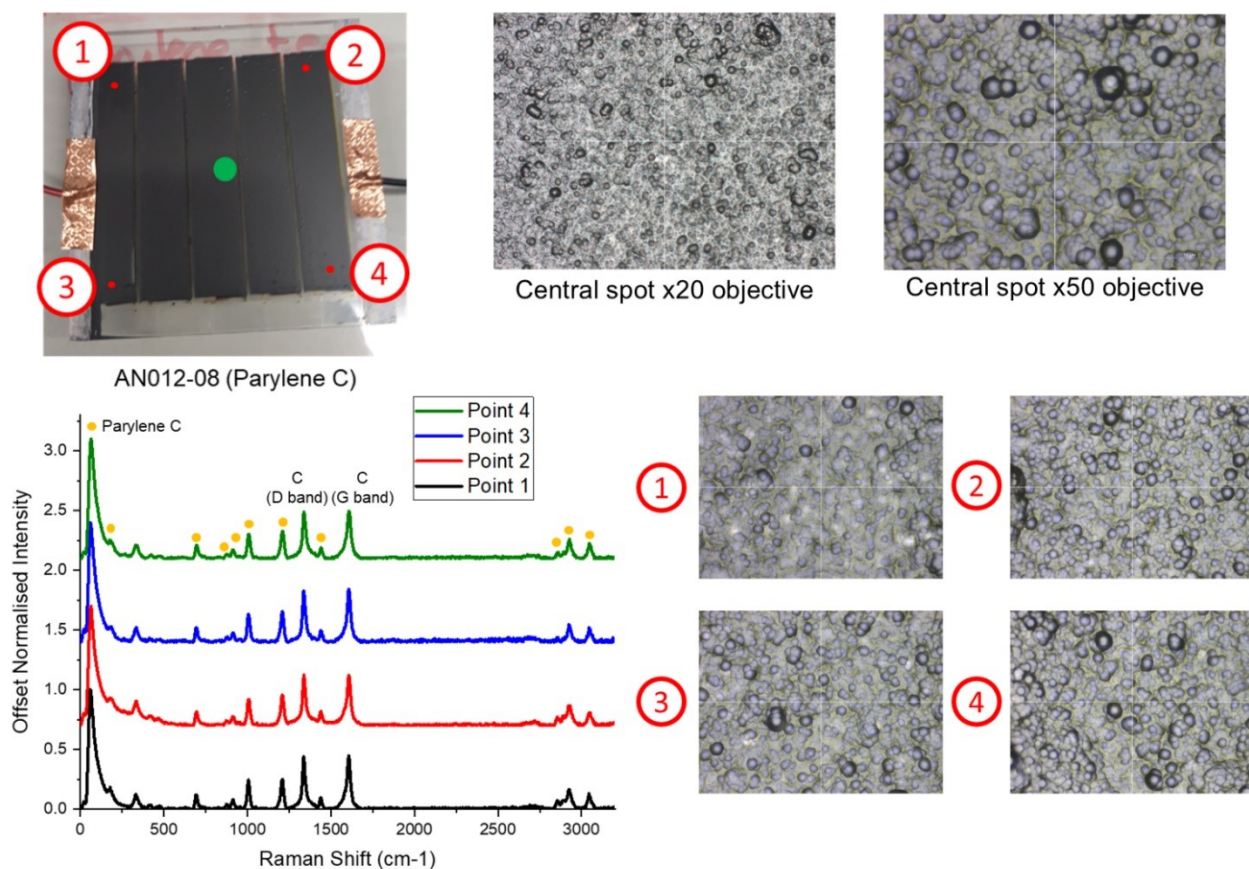


Figure S 6. Raman spectra and microscopy images at several points of a Parylene-C coated perovskite TMS minimodule.

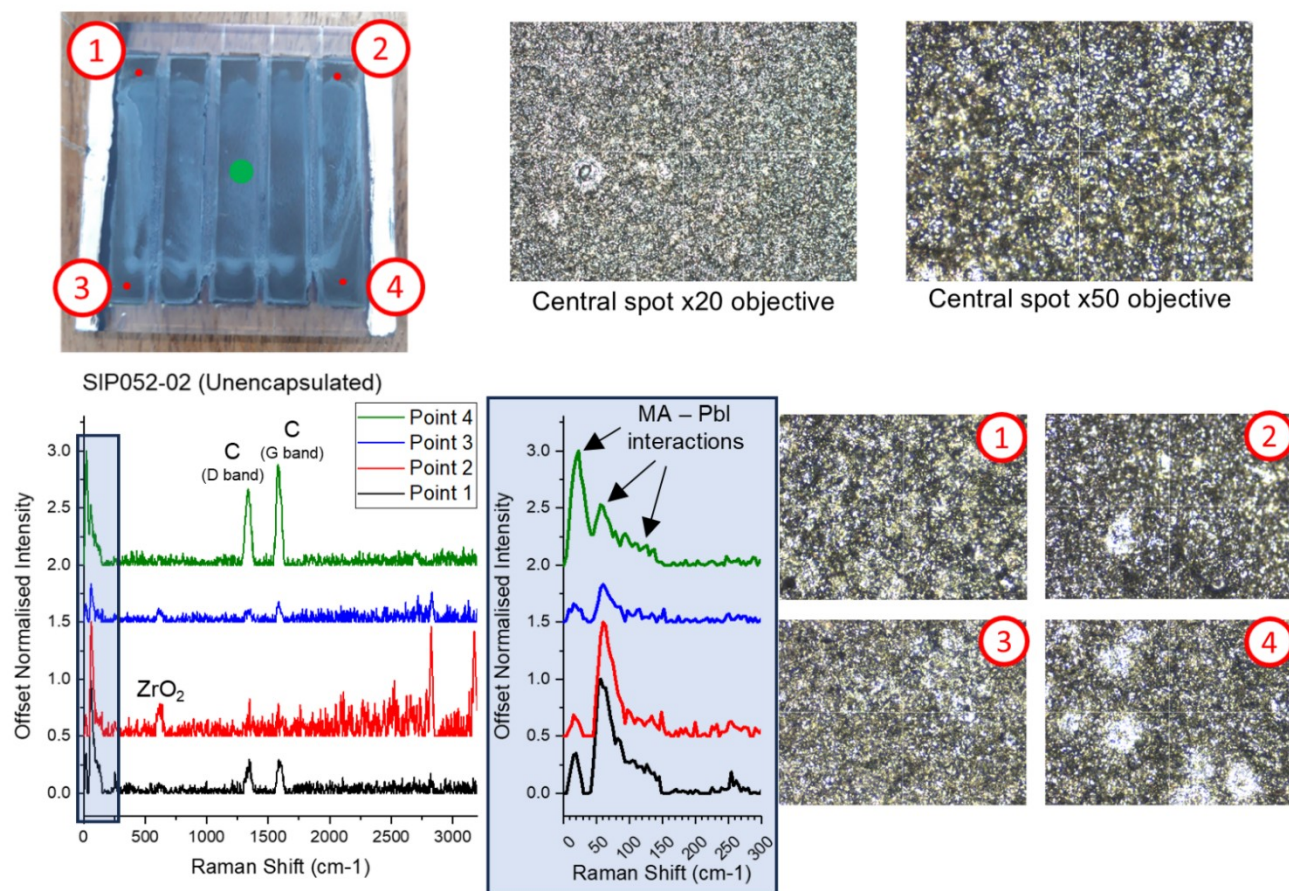


Figure S 7. Raman spectra and microscopy images at several points of an unencapsulated perovskite TMS minimodule.

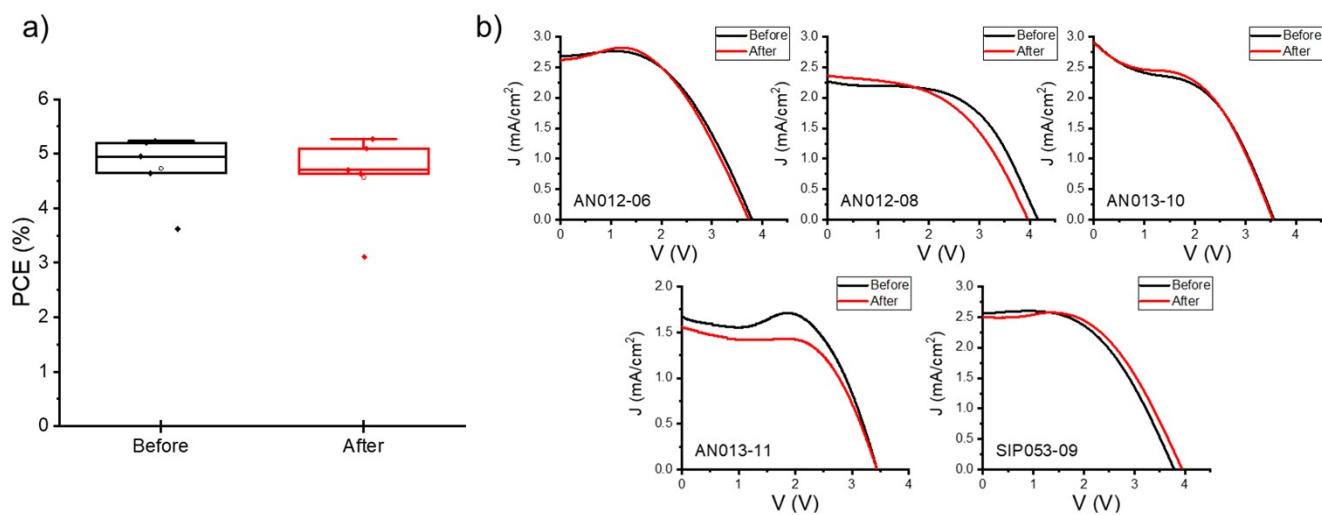


Figure S 8. PCE and JV scans before and after Parylene-C deposition on TMS minimodules.

Section 6. AFM Images.

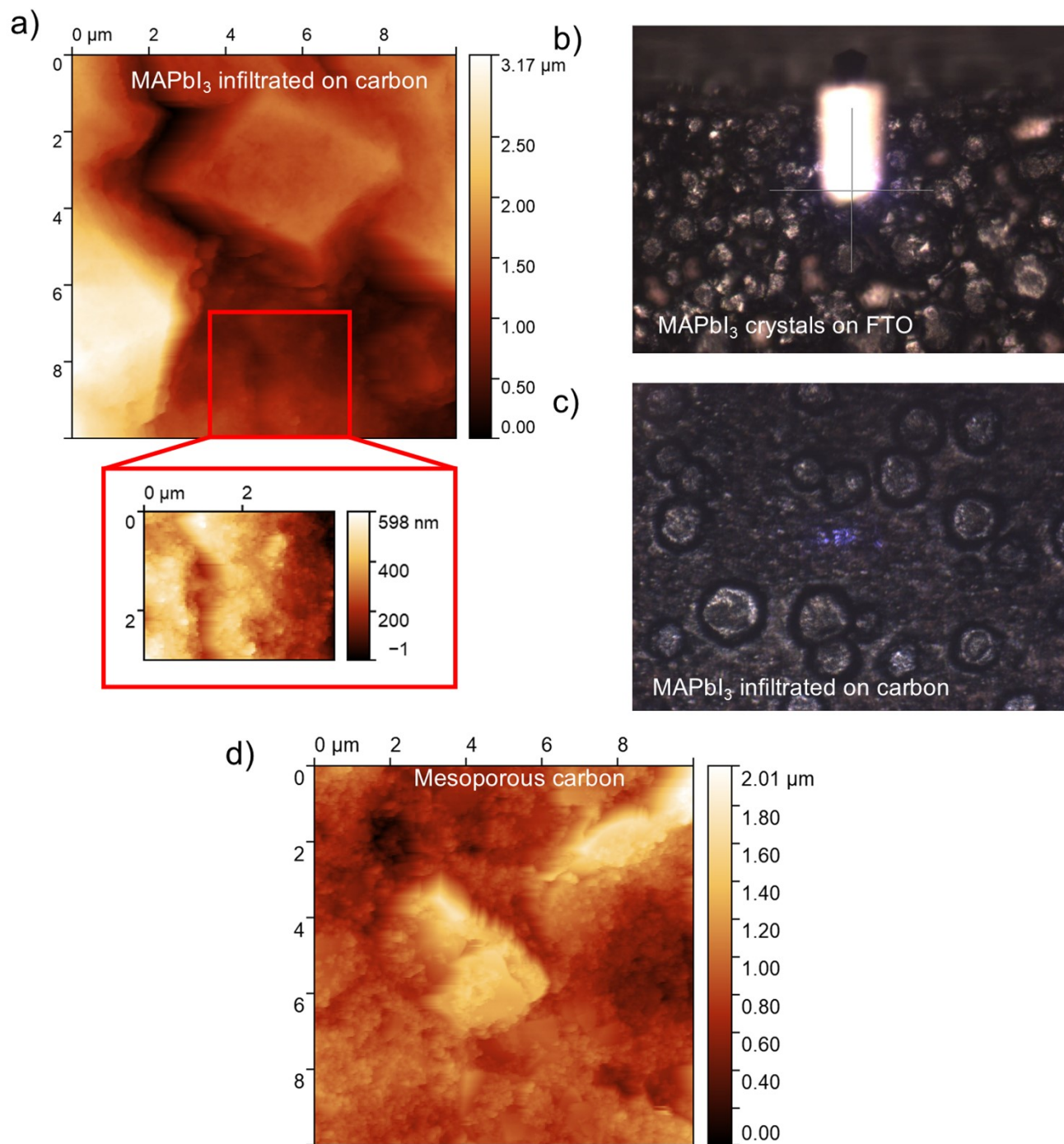


Figure S 9. a) AFM Scan of MAPbI₃ infiltrated on mesoporous carbon with sections of overfilling (top of image) and normal filling (inset). Microscope image of MAPbI₃ crystals on FTO (b) and infiltrated on mesoporous carbon (c). d) AFM image of mesoporous carbon layer.

Section 7. Environmental Conditions.

a)

2024																																																																																												
JANUARY							FEBRUARY							MARCH							APRIL							MAY							JUNE																																																									
M	Tu	W	Th	F	Sa	Su	M	Tu	W	Th	F	Sa	Su	M	Tu	W	Th	F	Sa	Su	M	Tu	W	Th	F	Sa	Su	M	Tu	W	Th	F	Sa	Su	M	Tu	W	Th	F	Sa	Su																																																			
1	2	3	4	5	6	7	8	9	10	11	12	13	14	15	16	17	18	19	20	21	22	23	24	25	26	27	28	29	30	31	1	2	3	4	5	6	7	8	9	10	11	12	13	14	15	16	17	18	19	20	21	22	23	24	25	26	27	28	29	30	31	1	2	3	4	5	6	7	8	9	10	11	12	13	14	15	16	17	18	19	20	21	22	23	24	25	26	27	28	29	30	31
8	9	10	11	12	13	14	15	16	17	18	19	20	21	22	23	24	25	26	27	28	29	30	31	1	2	3	4	5	6	7	8	9	10	11	12	13	14	15	16	17	18	19	20	21	22	23	24	25	26	27	28	29	30	31	1	2	3	4	5	6	7	8	9	10	11	12	13	14	15	16	17	18	19	20	21	22	23	24	25	26	27	28	29	30	31							
15	16	17	18	19	20	21	22	23	24	25	26	27	28	29	30	31	1	2	3	4	5	6	7	8	9	10	11	12	13	14	15	16	17	18	19	20	21	22	23	24	25	26	27	28	29	30	31	1	2	3	4	5	6	7	8	9	10	11	12	13	14	15	16	17	18	19	20	21	22	23	24	25	26	27	28	29	30	31														
22	23	24	25	26	27	28	29	30	31	1	2	3	4	5	6	7	8	9	10	11	12	13	14	15	16	17	18	19	20	21	22	23	24	25	26	27	28	29	30	31	1	2	3	4	5	6	7	8	9	10	11	12	13	14	15	16	17	18	19	20	21	22	23	24	25	26	27	28	29	30	31																					
29	30	31	26	27	28	29	25	26	27	28	29	30	31	29	30	27	28	29	30	31	20	21	22	23	24	25	26	27	28	29	30	31	24	25	26	27	28	29	30	30	31																																																			
JULY							AUGUST							SEPTEMBER							OCTOBER							NOVEMBER							DECEMBER																																																									
M	Tu	W	Th	F	Sa	Su	M	Tu	W	Th	F	Sa	Su	M	Tu	W	Th	F	Sa	Su	M	Tu	W	Th	F	Sa	Su	M	Tu	W	Th	F	Sa	Su	M	Tu	W	Th	F	Sa	Su																																																			
1	2	3	4	5	6	7	8	9	10	11	12	13	14	15	16	17	18	19	20	21	22	23	24	25	26	27	28	29	30	31	1	2	3	4	5	6	7	8	9	10	11	12	13	14	15	16	17	18	19	20	21	22	23	24	25	26	27	28	29	30	31																															
8	9	10	11	12	13	14	15	16	17	18	19	20	21	22	23	24	25	26	27	28	29	30	31	1	2	3	4	5	6	7	8	9	10	11	12	13	14	15	16	17	18	19	20	21	22	23	24	25	26	27	28	29	30	31																																						
15	16	17	18	19	20	21	22	23	24	25	26	27	28	29	30	31	1	2	3	4	5	6	7	8	9	10	11	12	13	14	15	16	17	18	19	20	21	22	23	24	25	26	27	28	29	30	31																																													
22	23	24	25	26	27	28	29	30	31	1	2	3	4	5	6	7	8	9	10	11	12	13	14	15	16	17	18	19	20	21	22	23	24	25	26	27	28	29	30	31																																																				
29	30	31	26	27	28	29	23	24	25	26	27	28	29	28	29	30	31	25	26	27	28	29	30	20	21	22	23	24	25	26	27	28	29	30	31	23	24	25	26	27	28	29	30	31																																																

 Left on the field
 Experiment 1: TMS minimodule Epoxi-glass Encapsulated
 Experiment 3: TMS minimodule POE-glass Encapsulated
B Measured
 Experiment 2: TMS solar cell Epoxi-glass Encapsulated (rCB)
 Experiment 4: TMS minimodule Parylene-C Encapsulated

b)

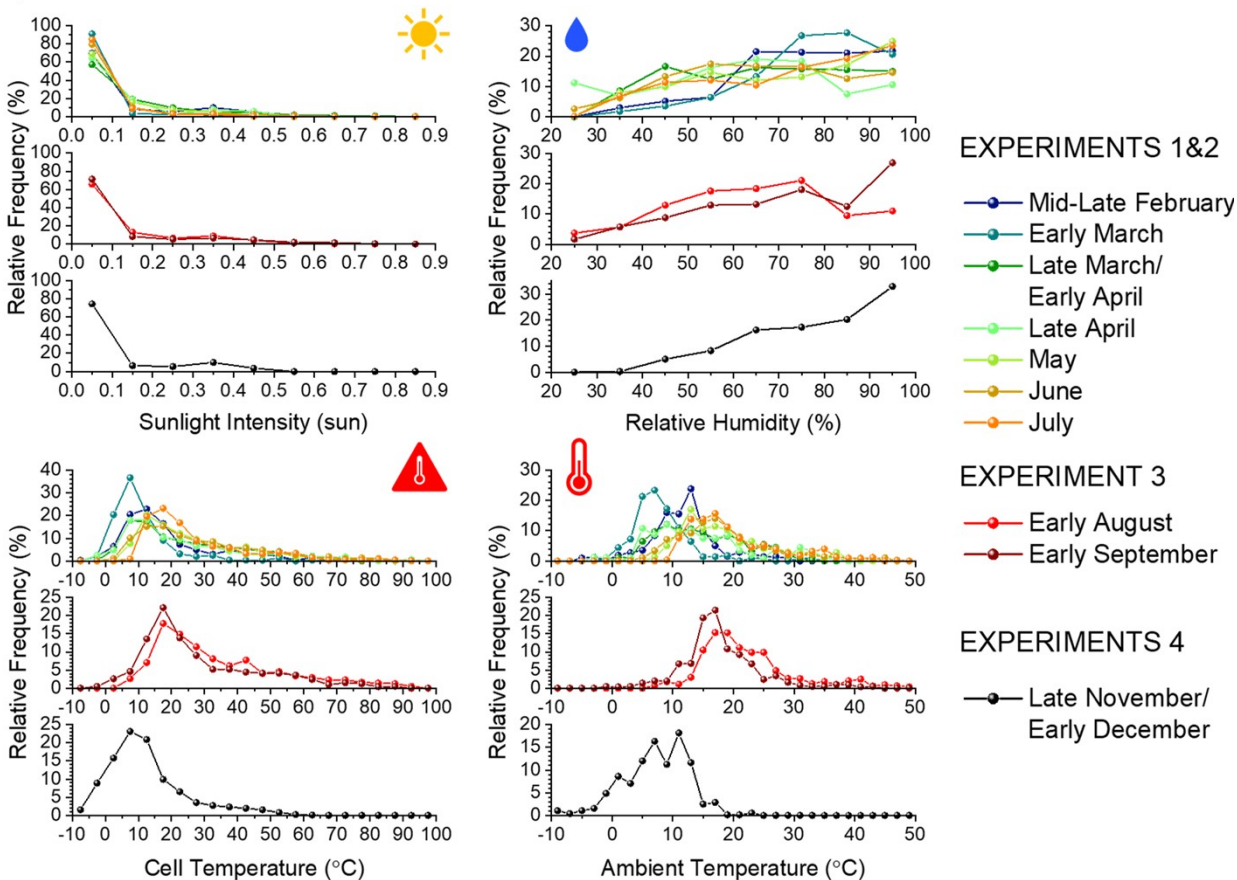


Figure S 10. a) Calendar with deployment times for the outdoor experiments. Coloured dates represent the days when cells were deployed on the field while dates in bold represent measurement dates. b)

Histogram of outdoor ambient conditions recorded during measurement periods highlighted in bold in a, including sunlight intensity, relative humidity, cell temperature and ambient temperature.

Measurement Period	T _{amb} (max) (°C)	T _{cell} (max) (°C)
Mid-Late February	28.8	71.51
Early March	32.6	73.69
Late March – Early April	32.6	71.75
Late April	37.7	93.82
May	40.4	91.72
June	45.9	88.95
July	47.1	91.72
Early August	49.4	93.82
Early September	42.3	88.56
Mid November – Early December	23.7	61.69

Table S 5. Maximum ambient and cell parameters recorded during outdoor measurement periods (following the calendar in Figure S 9a).

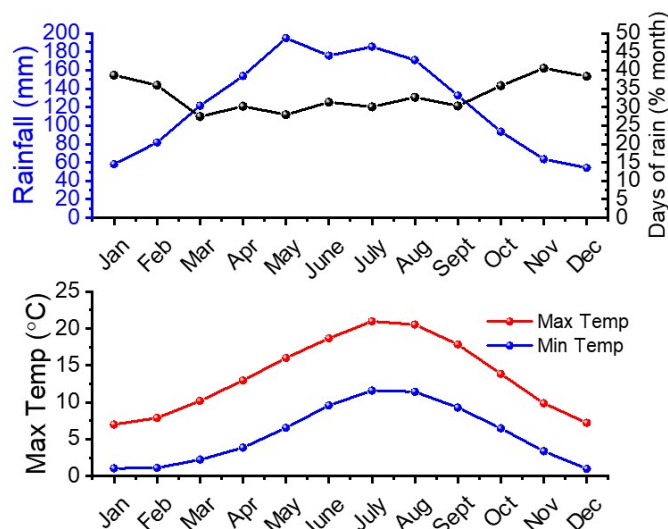


Figure S 11. Average historical weather data from Leeming Station (Met Office, 1991–2020)

Section 8. V_{OC} -to-RH relationship

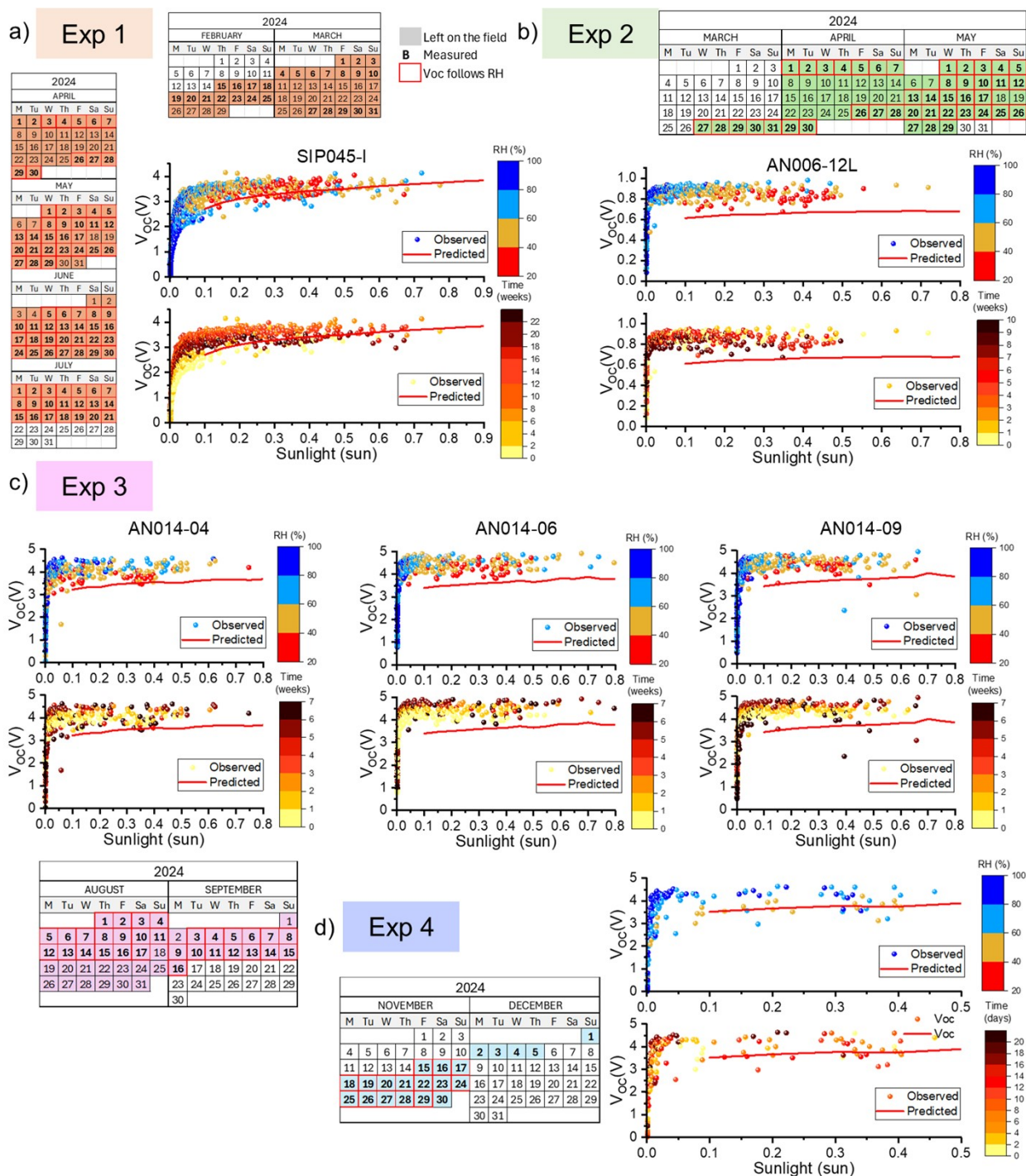


Figure S.12. Outdoor measurements of V_{OC} versus sunlight intensity for TMS devices in Experiments 1–4, shown in subplots (a)–(d). Each subplot contains two scatter plots with data points colour-mapped to represent time and relative humidity, respectively. A calendar highlighting the measurement dates accompanies each experiment.

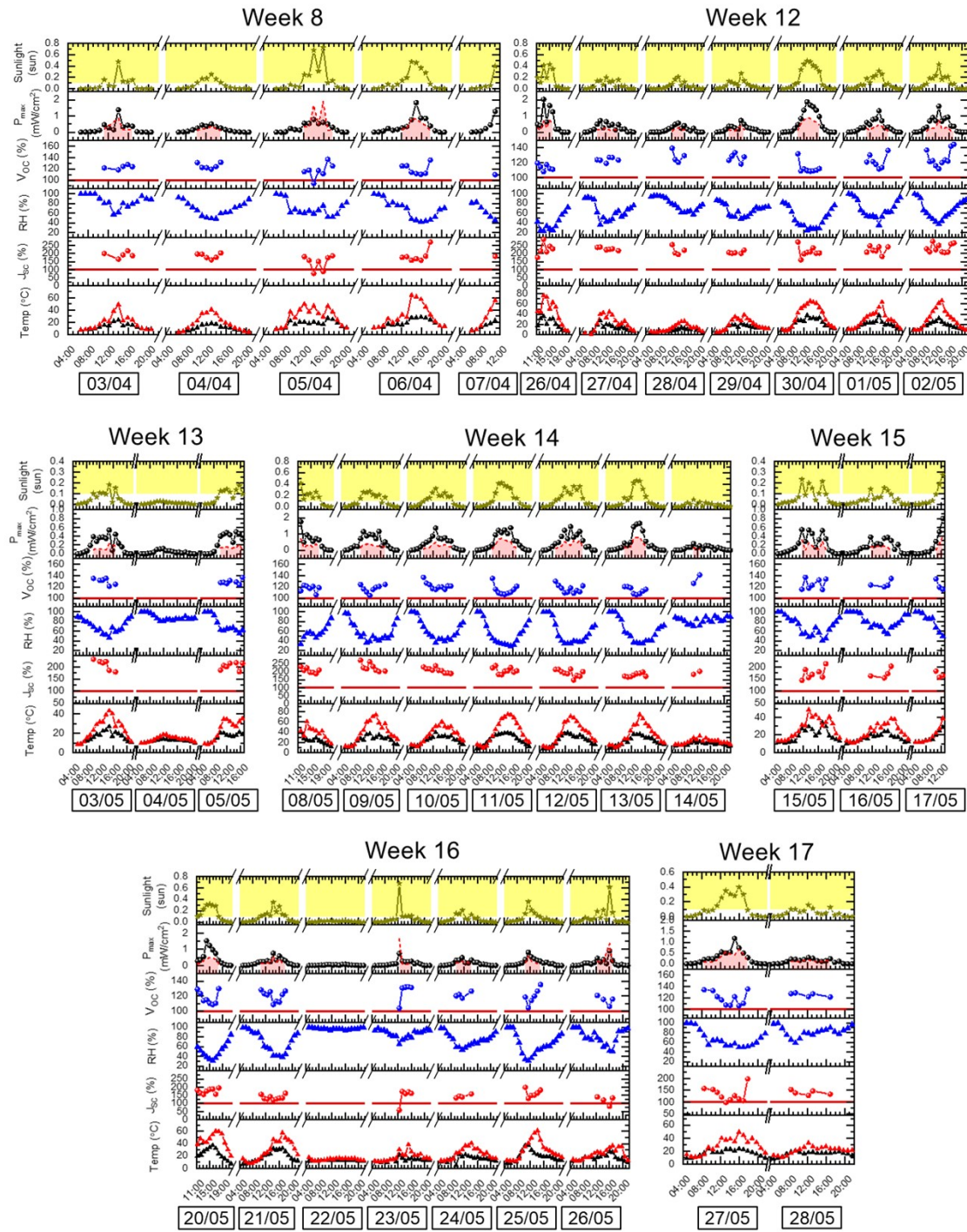


Figure S 13. Plot of ambient parameters (sunlight intensity, temperature and relative humidity) and device parameters overtime of SIP045-I between weeks 8 and 17 of the experiment where the V_{OC} -to-RH relationship is observed. These include the observed versus predicted maximum power and the change in V_{OC} and J_{SCin} regard to the device's initial calibration values.

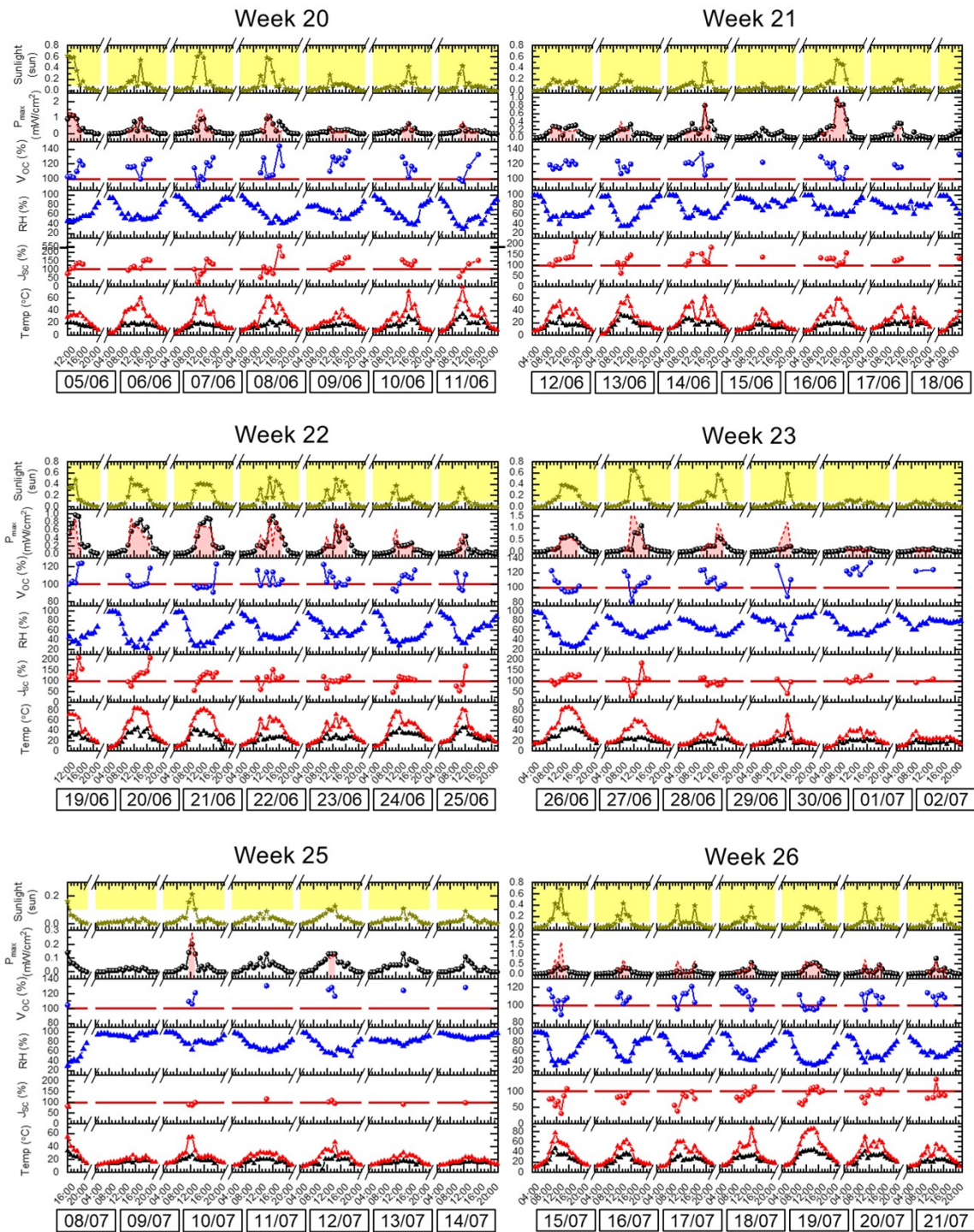


Figure S 14. Plot of ambient parameters (sunlight intensity, temperature and relative humidity) and device parameters overtime of SIP045-I between weeks 20 and 26 of the experiment where the V_{OC} -to-RH relationship is observed. These include the observed versus predicted maximum power and the change in V_{OC} and J_{SC} in regard to the device's initial calibration values.

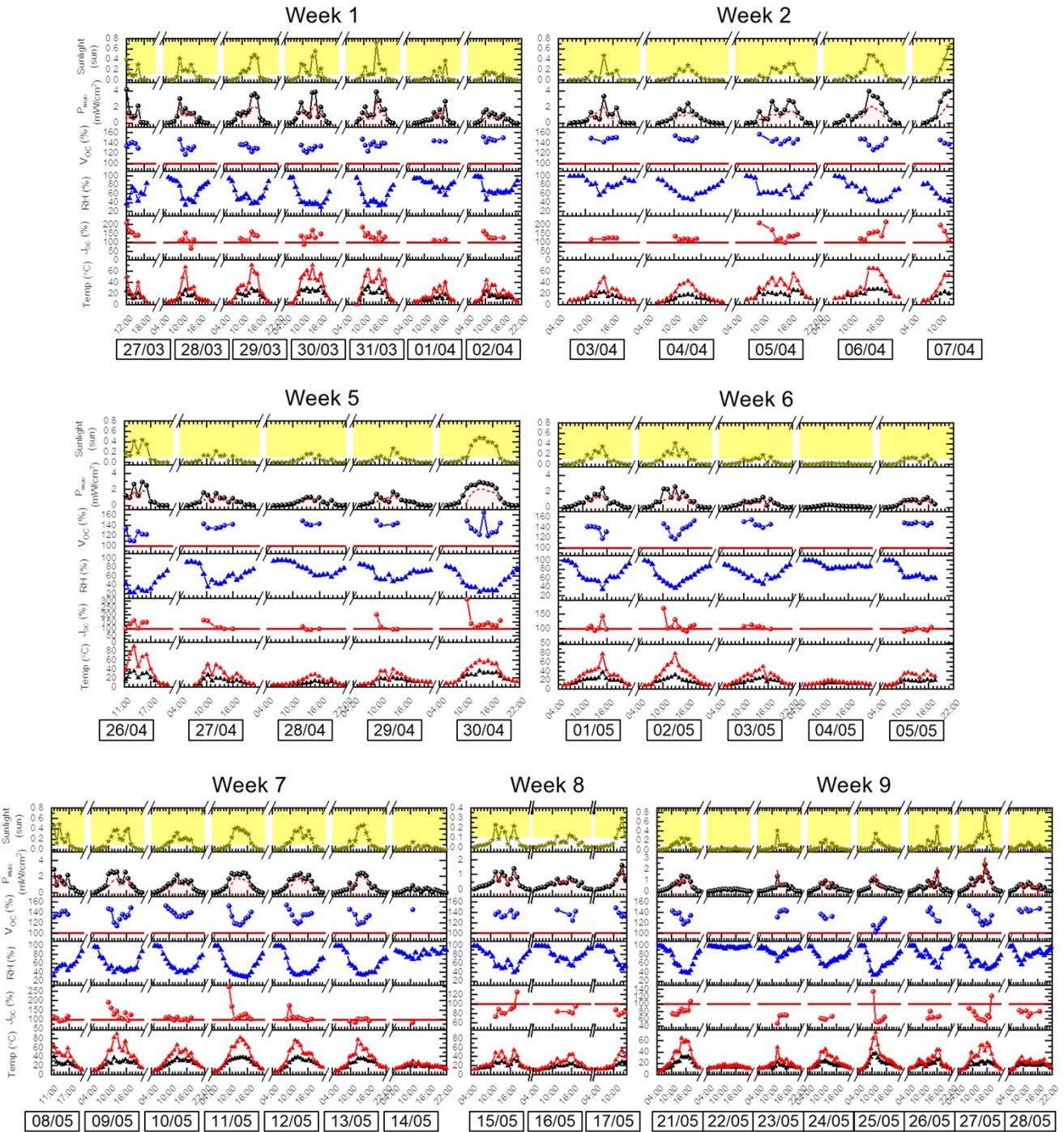


Figure S 15. Plot of ambient parameters (sunlight intensity, temperature and relative humidity) and device parameters overtime of AN006-12L between weeks 1 and 9 of the experiment where the V_{OC} -to-RH relationship is observed. These include the observed versus predicted maximum power and the change in V_{OC} and J_{SC} in regard to the device's initial calibration values.

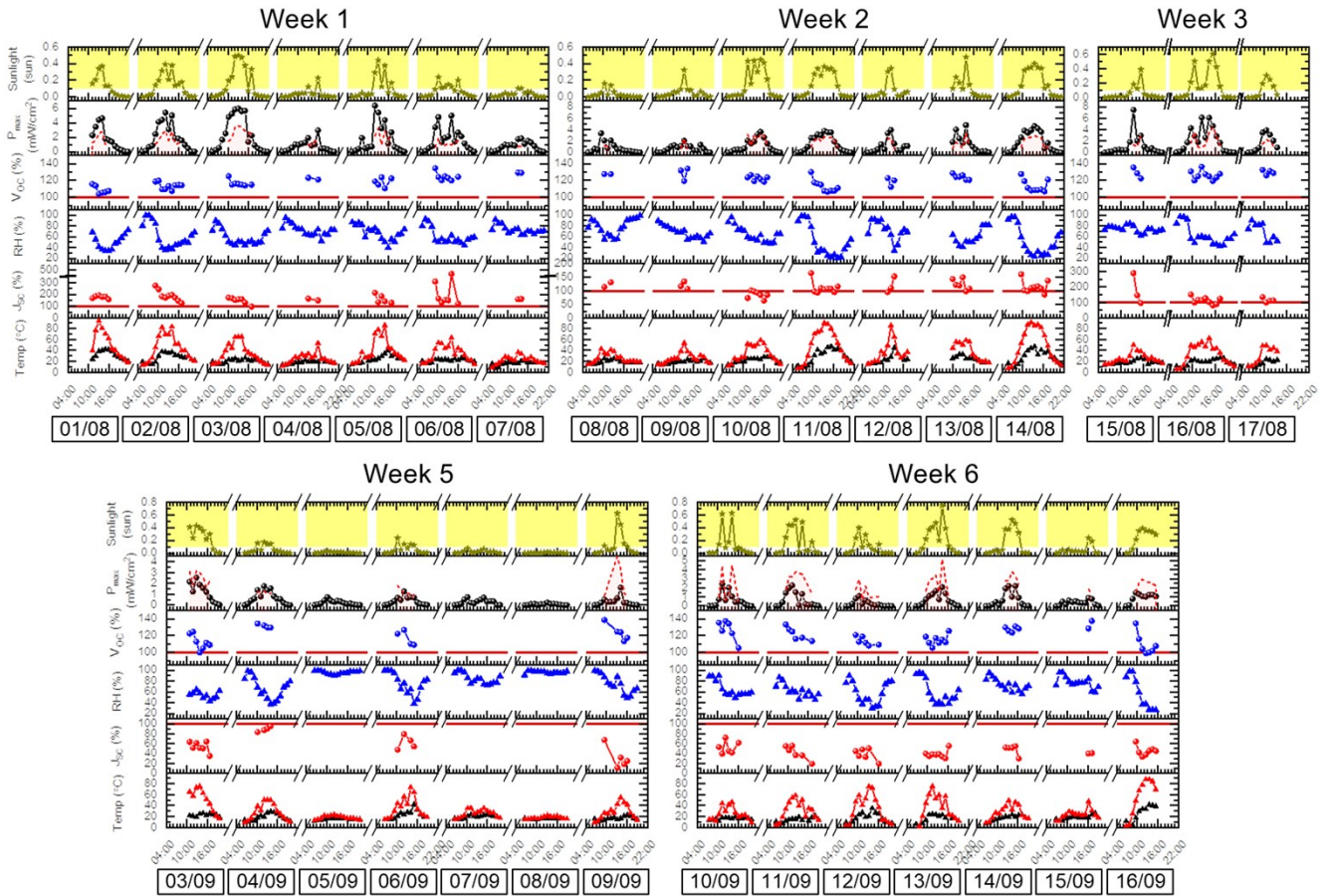


Figure S 16. Plot of ambient parameters (sunlight intensity, temperature and relative humidity) and device parameters overtime of AN014-04 between weeks 1 and 6 of the experiment where the V_{OC} -to-RH relationship is observed. These include the observed versus predicted maximum power and the change in V_{OC} and J_{SC} in regard to the device's initial calibration values.

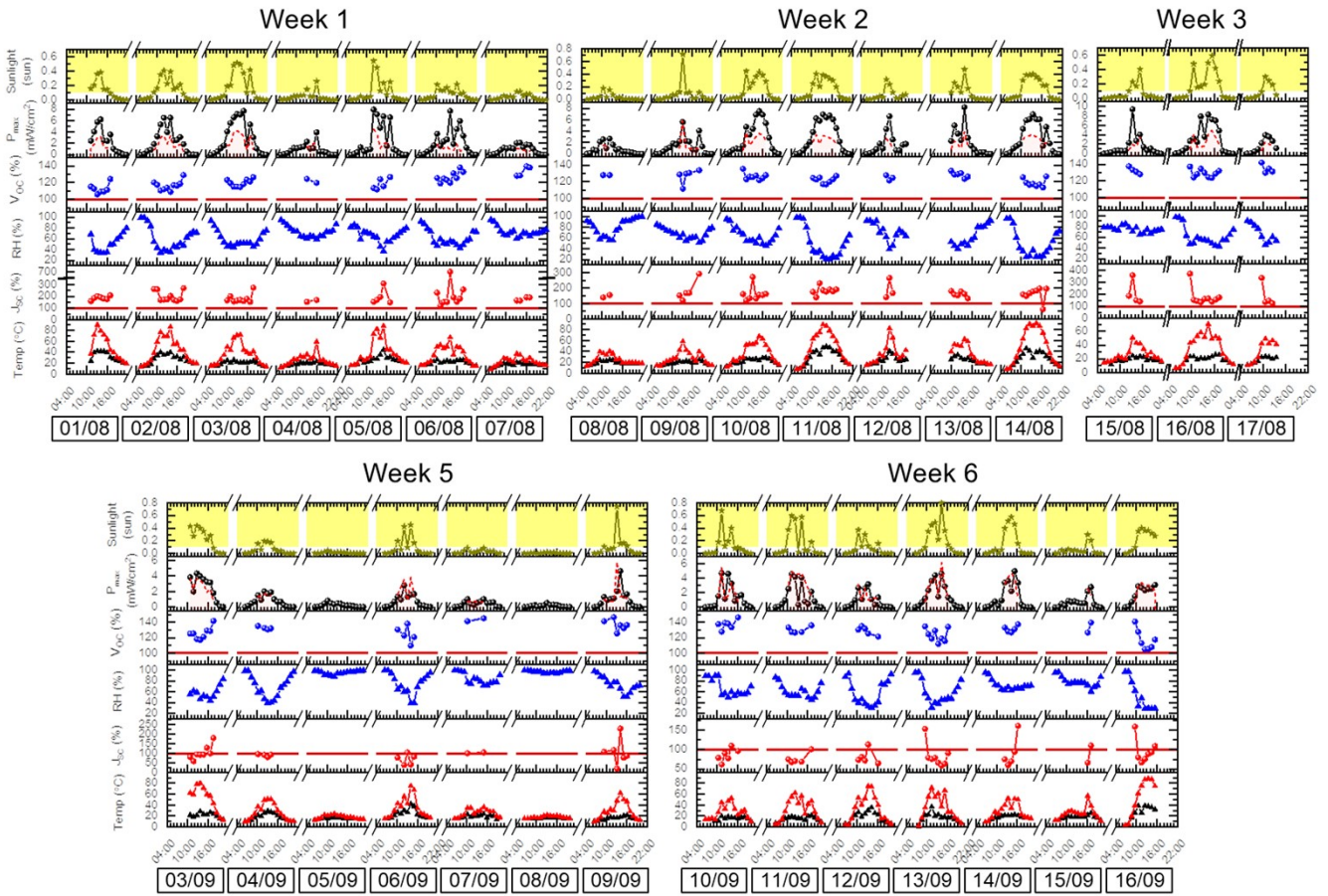


Figure S 17. Plot of ambient parameters (sunlight intensity, temperature and relative humidity) and device parameters overtime of AN014-06 between weeks 1 and 6 of the experiment where the V_{OC} -to-RH relationship is observed. These include the observed versus predicted maximum power and the change in V_{OC} and J_{SC} in regard to the device’s initial calibration values.

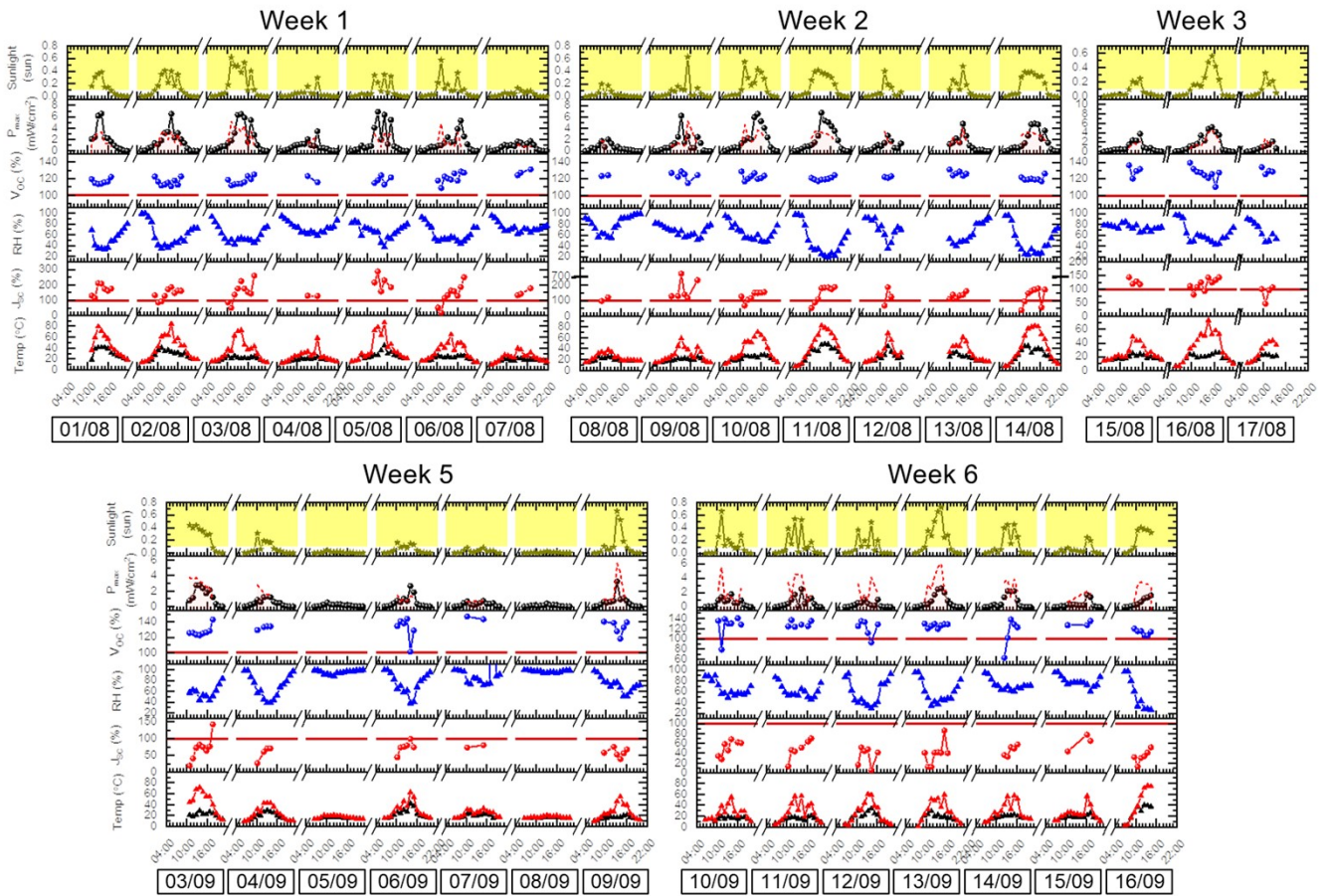


Figure S 18. Plot of ambient parameters (sunlight intensity, temperature and relative humidity) and device parameters overtime of AN014-09 between weeks 1 and 6 of the experiment where the V_{OC} -to-RH relationship is observed. These include the observed versus predicted maximum power and the change in V_{OC} and J_{SC} in regard to the device's initial calibration values.

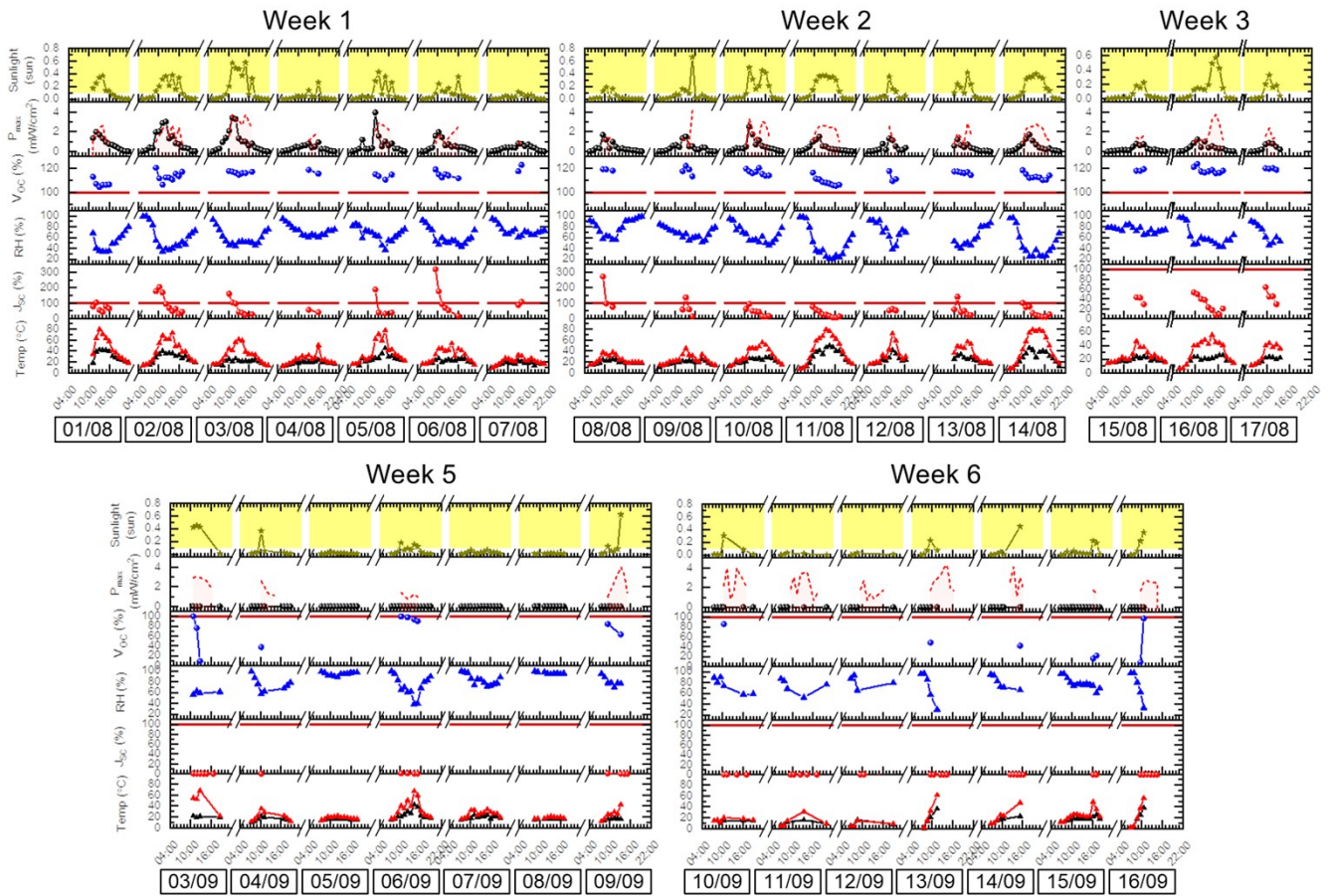


Figure S 19. Plot of ambient parameters (sunlight intensity, temperature and relative humidity) and device parameters overtime of AN014-12 between weeks 1 and 6 of the experiment where the V_{OC} -to-RH relationship is observed. These include the observed versus predicted maximum power and the change in V_{OC} and J_{SC} in regard to the device's initial calibration values.

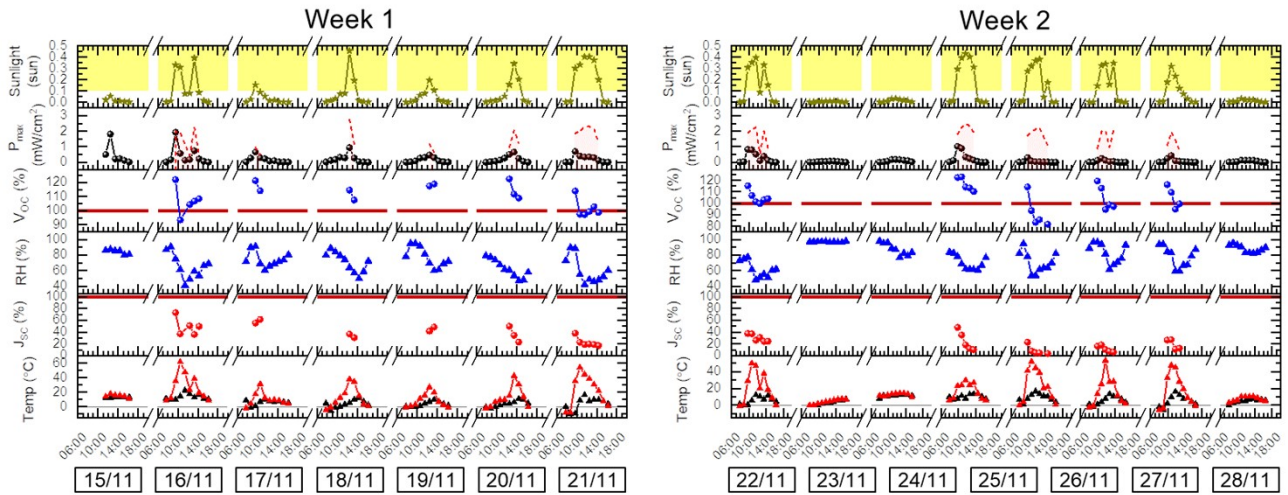


Figure S 20. Plot of ambient parameters (sunlight intensity, temperature and relative humidity) and device parameters overtime of SIP053-09 between weeks 1 and 2 of the experiment where the V_{OC} -to-RH relationship is observed. These include the observed versus predicted maximum power and the change in V_{OC} and J_{SC} in regard to the device's initial calibration values.

Section 9. Lab Hydration and Dehydration experiments

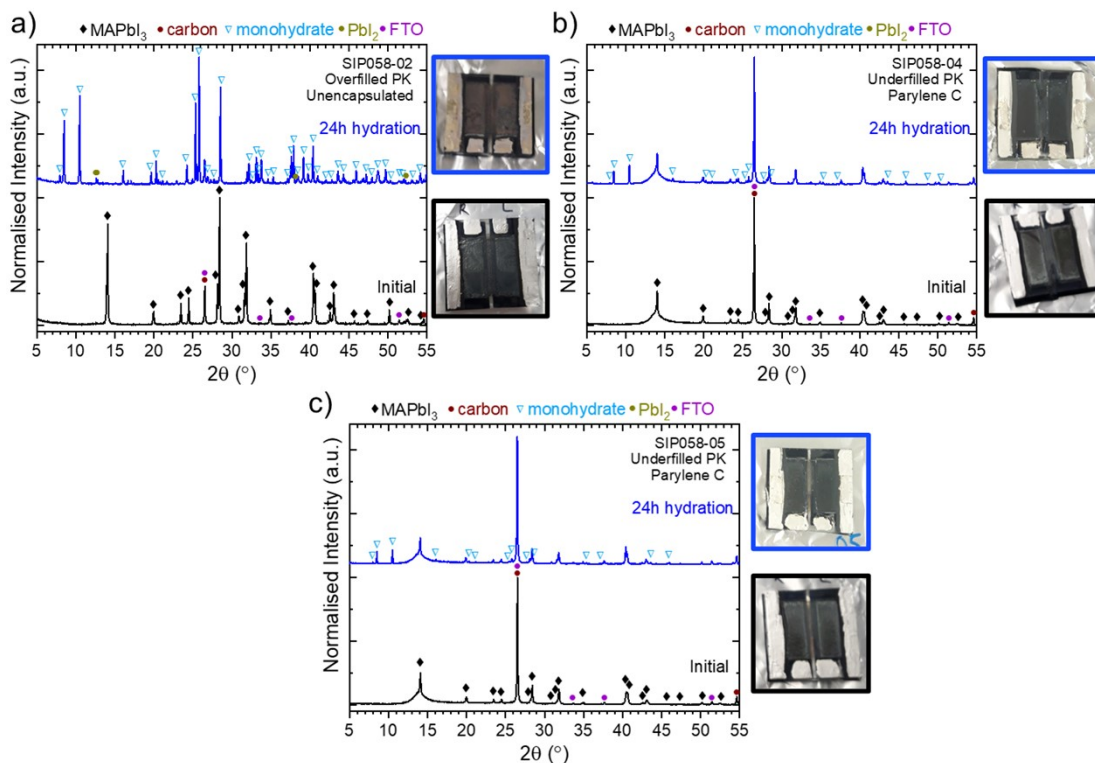


Figure S 21. XRD scans before and after hydration of unencapsulated (a, c) and Parylene-C coated (b) TMS solar cells before and after 24h in a high humidity environment (RH>90%).

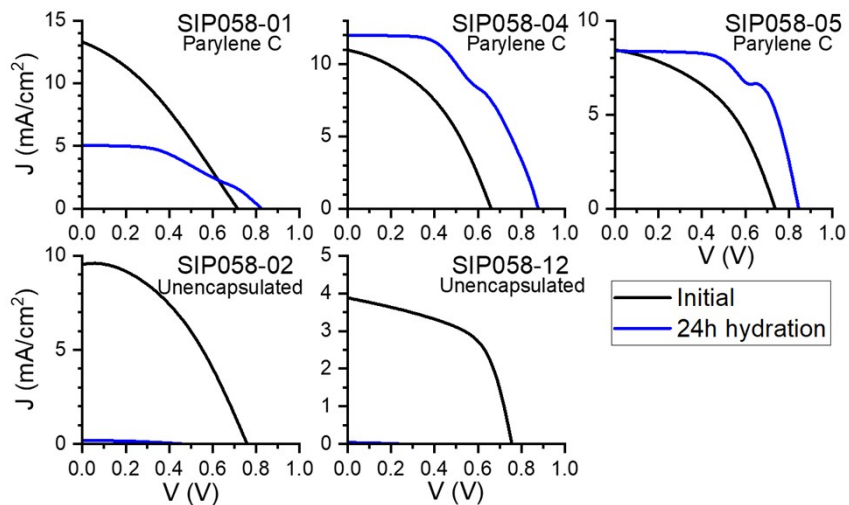


Figure S 22. Reverse JV scans of unencapsulated and Parylene-C coated TMS hydrated solar cells before and after exposure to a high humidity environment (RH>90%) for 24h.

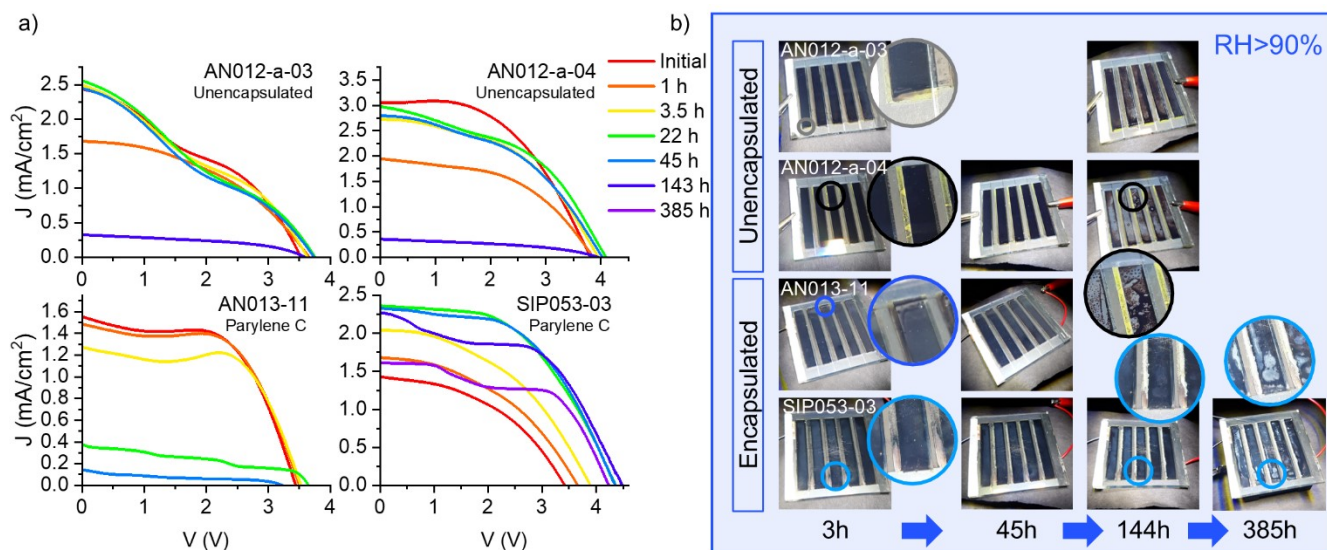


Figure S 23. Reverse JV scans (a) and images (b) of unencapsulated and Parylene-C coated TMS hydrated minimodules before and after exposure to a high humidity environment (RH>90%) for increasing times.

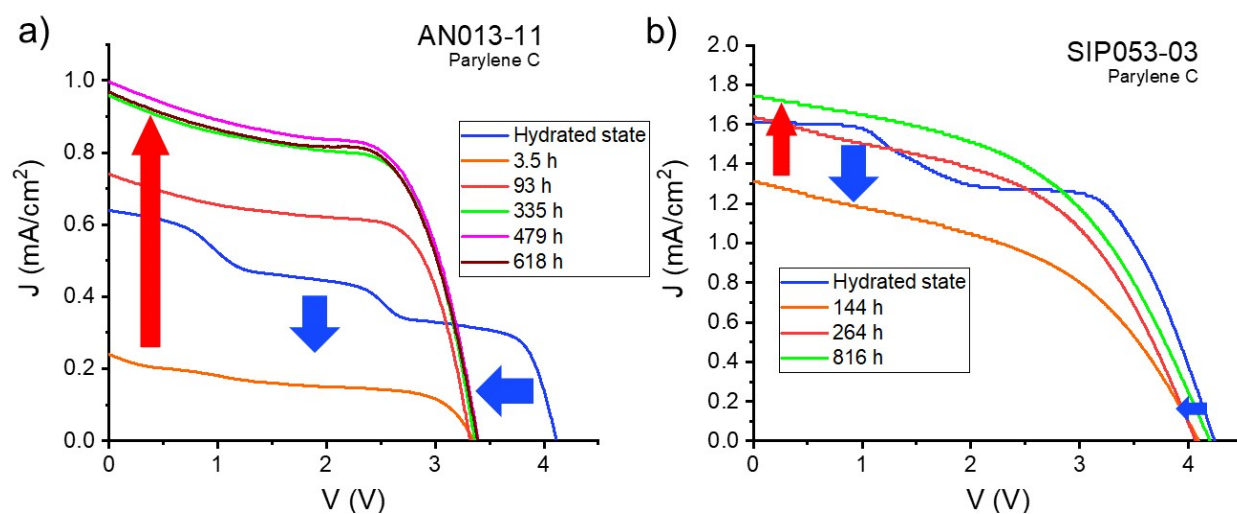


Figure S 24. Reverse JV scans of AN013-11 (a) and SIP05303 (b) Parylene-C coated TMS hydrated minimodules before and after up to 618 h and 816h of exposure to 40-50°C in an oven.

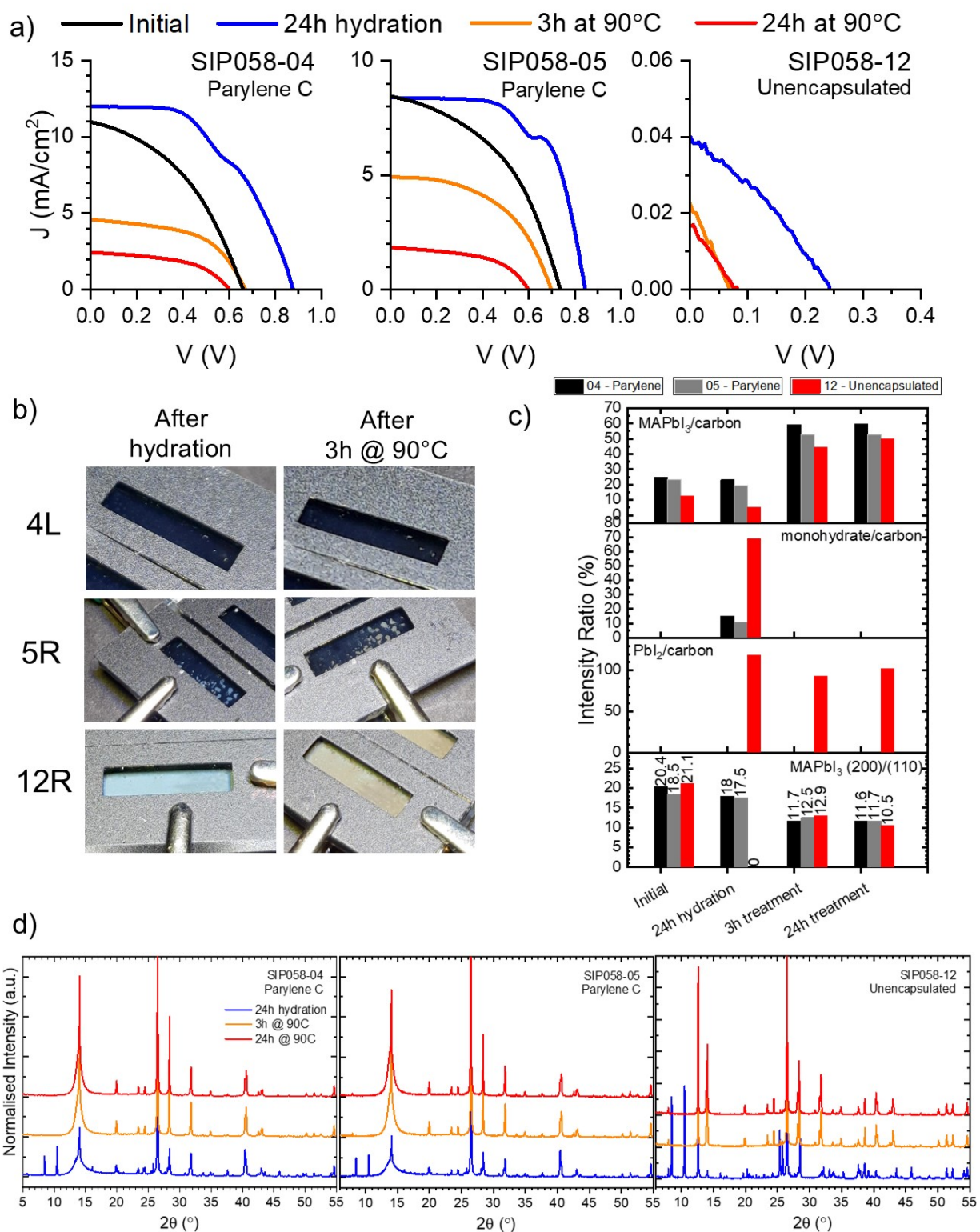


Figure S 25. Reverse JV scans (a), images (b), XRD scans (d) and XRD peak ratios (c) of unencapsulated and Parylene-C coated TMS hydrated solar cells before and after up to 24h of exposure to 90°C in an oven.

Sample	Encapsulant	Treatment	Weight (3h recovery) (g)	Weight (24h recovery) (g)
SIP058-01	Parylene-C	Vacuum	7.2163	7.2163
SIP058-02	None	Vacuum	7.2668	7.2668
SIP058-04	Parylene-C	90 °C	7.0368	7.0368
SIP058-05	Parylene-C	90 °C	7.3953	7.3948
SIP058-12	None	90 °C	6.8528	6.8523

Table S 6. Weight change of TMS hydrated solar cells after 3h and 24h of exposure to vacuum and temperature recovery treatments.

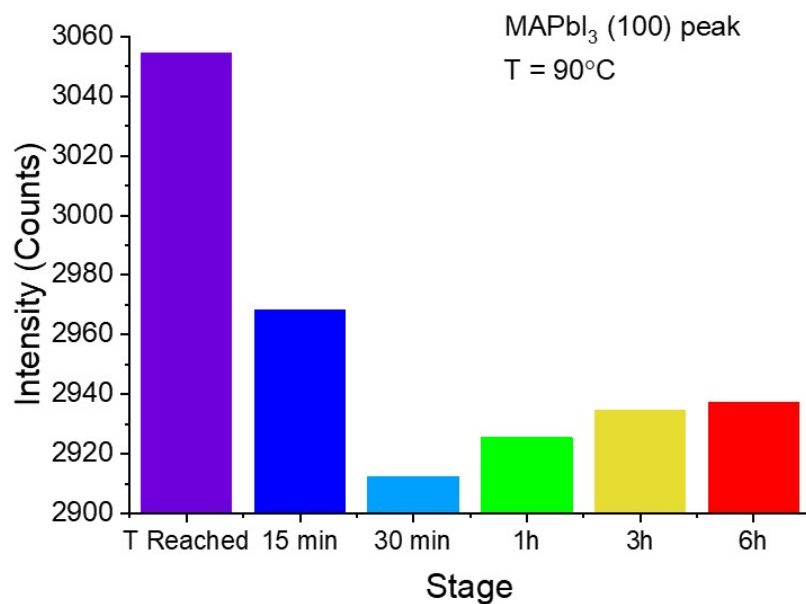


Figure S 26. Peak height of the cubic MAPbI₃ (100) plane during the in-situ XRD experiment at 90 °C.

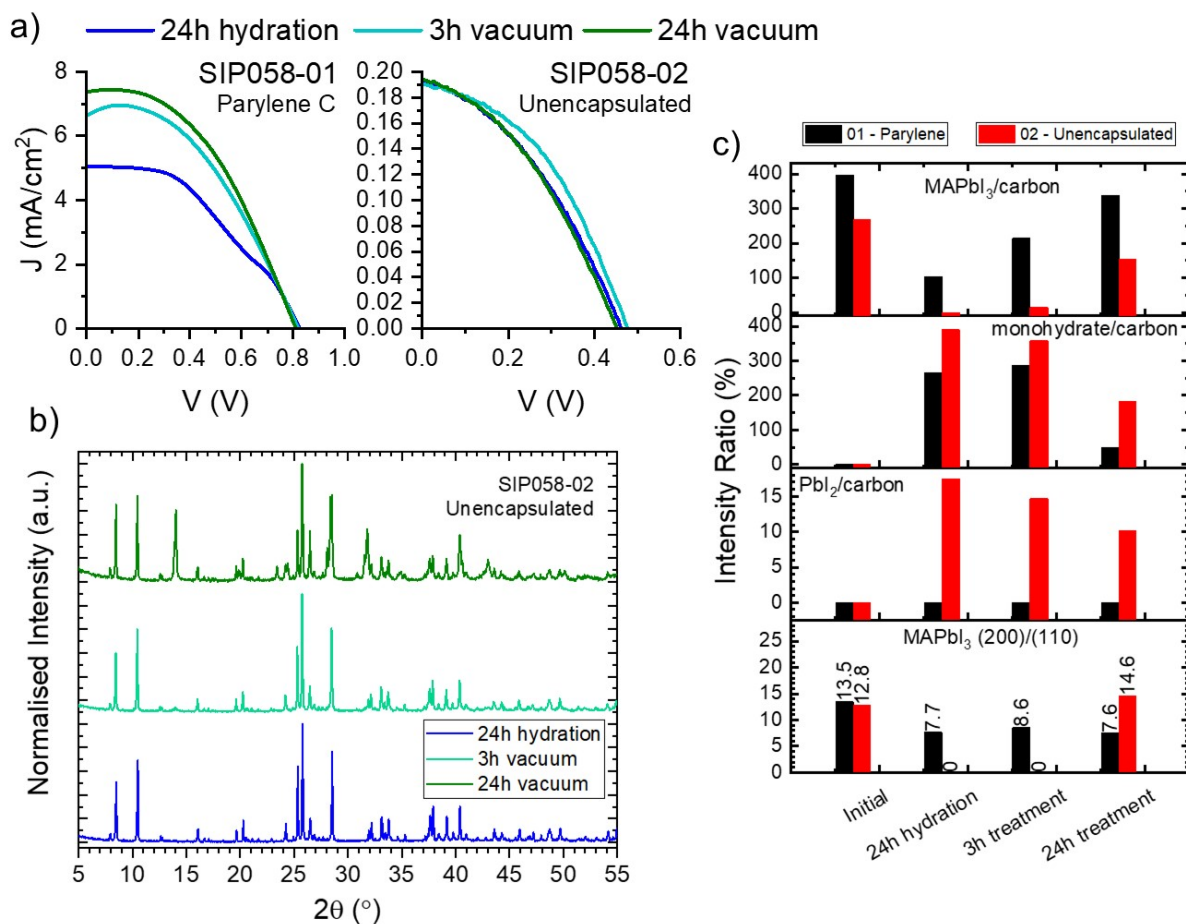


Figure S 27. Reverse JV scans (a), XRD scans (c) and XRD peak ratios (b) of unencapsulated and Parylene-C coated TMS hydrated solar cells before and after up to 24h of exposure to vacuum in a desiccator.

References

- (1) Babin, M.; Eder, G. C.; Voronko, Y.; Oreski, G. Water Vapor Permeability of Polymeric Packaging Materials for Novel Glass-free Photovoltaic Applications. *J Appl Polym Sci* 2024, 141 (31). <https://doi.org/10.1002/app.55733>.
- (2) *Araldite Rapid Syringe Epoxy | NWT4471P | Glues & Adhesives*. <https://www.officestationery.co.uk/product/araldite-rapid-syringe-epoxy-adhesive-24ml-pack-6-nwt4471p-NWT4471P/> (accessed 2025-03-12).
- (3) The Compound Company. *SAFETY DATA SHEET: Yparex - Silane Functionalised Polymer Film*; 2021.
- (4) SCS Speciality Coating Systems. *Does Parylene make my Product Waterproof?* <https://scscoatings.com/newsroom/blog/does-parylene-make-my-product-waterproof/#:~:text=February%2016%2C%202021,Chaotic%20weather> (accessed 2025-07-01).
- (5) SCS Specialty Coating Systems. *A Guide to Parylene Service Temperatures*. <https://scscoatings.com/newsroom/blog/a-guide-to-parylene-service-temperatures/#:~:text=Because%20oxygen%2Dfree%20environments%20prohibit,to%20using%20major%20Parylene%20types>. (accessed 2025-07-01).